AAS 12-169

A NEW METHOD FOR SIMULATING THE ATTITUDE DYNAMICS OF PASSIVELY MAGNETICALLY STABILIZED SPACECRAFT

Roland Burton[*], Joseph Starek[†], and Stephen Rock[‡]

A new method for simulating the behavior of magnetically permeable material is presented that offers an order of magnitude reduction in simulation run time compared to existing methods with no loss in accuracy. The new method was integrated into a full attitude dynamics simulation of the NASA O/OREOS spacecraft and preliminary comparisons between the simulation results and orbit data are made.

INTRODUCTION

Many nano satellites, including the ARC 3U family of buses, use passive magnetic attitude stabilization systems consisting of a combination of permanent dipoles and magnetically permeable material. Permanent dipoles are used to align a spacecraft axis to the local magnetic field vector and the permeable material is used to provide damping and remove excessive post-separation attitude rates.

There is a desire to accurately simulate the transient behavior of such passively magnetically stabilized spacecraft both during the initial post separation phase and when subjected to disturbances during the mission. Initial post separation tumbling rates can be of the order of several degrees a second requiring integration time steps of less than a second to preserve numerical accuracy. As spacecraft are typically lightly damped, this post separation de-tumbling phase can take several days to complete. The combination of a multiple day time horizon and sub second time steps necessitates the evaluation of millions of time steps for accurate simulations, and existing methods can take several hours to complete. Any improvement in simulation speed will allow for more initial conditions, disturbances and design parameters to be studied. Simulation speed increases would be especially beneficial when performing parameter identification, an iterative process requiring large numbers of simulation runs.

This paper presents a new method of numerically integrating the differential equations commonly used to describe the hysteresis behavior of magnetically permeable materials that offers an order of magnitude decrease in the computational time with no loss in accuracy. The computational speed advantage is retained when the magnetic model is integrated into a full spacecraft attitude simulation. The new method was integrated into a full attitude simulation of the O/OREOS spacecraft which was a 3U nano satellite launched in November 2010.

---

[*] Stanford University and NASA Ames Research Center

[†] Stanford University and NASA Ames Research Center

[‡] Professor, Stanford University.

BACKGROUND

If a permeable rod is placed in a time varying magnetic field, the flux density induced in the rod is seen to lag changes in the external field, a phenomenon known as hysteresis. A typical hysteresis loop is shown in Figure 1. The saturation, B_s, is the maximum induced magnetic flux density that the rod can support. The coercivity, H_c, is the strength of the external magnetic field required to reverse the direction of the flux induced in the rod. Finally the remanence, B_r, is the residual flux density remaining in the rod once the external field is removed. A permeable rod set to spin in a magnetic field generates heat as a result of internal friction due to the movement of magnetic domains within the rod. The heat energy is transferred from kinetic energy, and absent other torques the rod will slow down. The energy loss, ΔE_h, for a rod of volume V over one cycle is given by

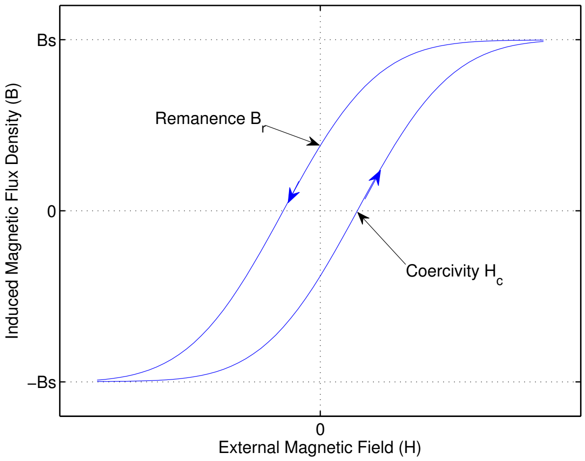

Figure 1. Typical Hysteresis Loop

$$\Delta E_h = V \oint H dB \tag{1}$$

where the circular integral is taken over one closed loop of changes in external magnetic field H and induced magnetic flux density B.

Magnetically permeable rods have been used to damp the angular motions of earth orbiting satellites since the earliest launches of the 1960s. The early analysis[1] of hysteresis material used for passive damping focused on ensuring the energy loss per loop was sufficient to reduce post-separation spin rates in a suitable time frame and did not consider the behavior within the loop in detail. Flatley and Henretty[2] introduced an empirically derived closed form model to describe the bounding curves of the hysteresis loops as illustrated in Figure 2, and the behavior within the loop. The Flatley and Henretty model has been widely used in the subsequent literature. The model approximates the bounds of the hysteresis loop to an inverse tangent function, described by the equivalent empirical relationships:

$$B_{lim}(H) = B_s \left(\frac{2}{\pi}\right) \arctan\left(k(H \pm H_c)\right) \tag{2}$$

$$H_{lim}(B) = \frac{1}{k} \tan\left(\frac{\pi}{2}\frac{B}{B_s}\right) \pm H_c \tag{3}$$

where the shaping factor, k, is defined as

$$k = \frac{1}{H_c} \tan\left(\frac{\pi}{2}\frac{B_r}{B_s}\right) \tag{4}$$

In Equation (2) H is the applied external magnetic field and B_{lim} is the limiting value of the induced magnetic flux within the material. The shape of the loop is controlled by the material properties of coercivity H_c, saturation B_s, and remanence, B_r as shown in Figure 2. It can be shown that for this empirical model

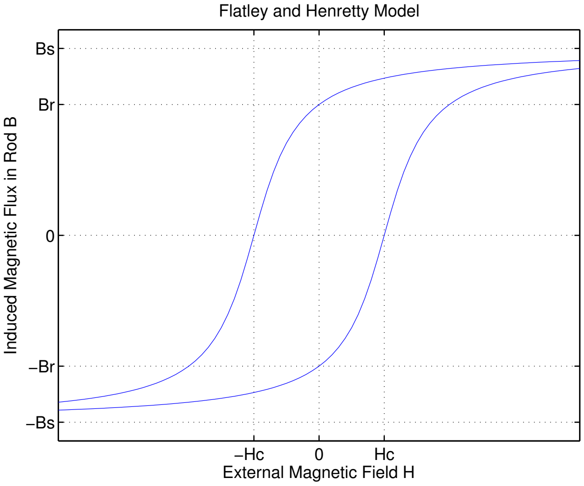

Figure 2. Magnetic Hysteresis Loop Model

$$\oint H dB = 4B_s H_c \tag{5}$$

and the maximum energy loss over a full cycle is given by

$$\Delta E_h = 4VB_sH_c \tag{6}$$

The slope of either boundary curve as a function of the induced flux B is given by

$$\frac{dB_{lim}}{dH} = \frac{2}{\pi} k B_s \cos^2\left(\frac{\pi}{2}\frac{B}{B_s}\right) \tag{7}$$

and behavior within the loop could reasonably be modeled by

$$\frac{dB}{dH} = \left[q_0 + (1 - q_0) f^p\right] \frac{dB_{lim}}{dH} \tag{8}$$

where p and q_0 are determined empirically from testing the material, and f is the fractional distance to the limiting boundary condition. Subsequent implementations in full spacecraft simulations[3,4] have used $p = 2$ and $q_0 = 0$, leading to the ordinary differential equation

$$\frac{dB}{dH} = \frac{2}{\pi} k B_s \cos^2\left(\frac{\pi}{2}\frac{B}{B_s}\right) \left(\frac{H - H_{lim}(B)}{2H_c}\right)^2 \tag{9}$$

which can be numerically integrated in a time varying external magnetic field H using the relationship

$$\frac{dB}{dt} = \frac{dB}{dH}\frac{dH}{dt} \tag{10}$$

In Equation (9) the left boundary is used to compute $H_{lim}(B)$ when H is increasing, and the right boundary when H is decreasing. Sample results from numerically integrating Equation (10) are illustrated in Figure 3, where a stationary rod was simulated in a sinusoidal external field from an initial condition $H = B = 0$. Figure 3(a) illustrates the trajectory when the maximum external field is insufficient to achieve saturation. In Figure 3(b) the external field is sufficient to achieve saturation, and the loop boundaries are traced once initially reached.

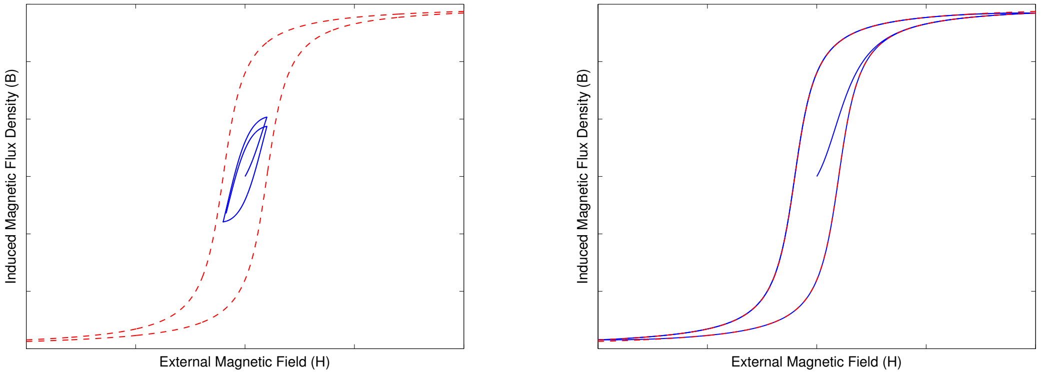

(a) $H = H_c \sin\omega t$ (b) $H = 10H_c \sin\omega t$

Figure 3. Induced flux density loops in a sinusoidal external field

Care must be taken when numerically integrating Equation (10). Fixed step integration methods will not guarantee the induced magnetic flux B will be bounded between the curves, and can cause B to exceed B_s, leading to evaluation errors in subsequent steps. A simple remedy is to bound the solution using Equation (2) after every time step. While this bounding step ensures that the solution remains within the hysteresis loop, it is inelegant and adds additional computational burden as two additional trigonometric function calls must be made each time the differential equation is integrated.

NEW METHOD

The new alternative approach suggested here introduces the substitution

$$S = \tan\left(\frac{\pi}{2}\frac{B}{B_s}\right) \tag{11}$$

to reduce the boundary equations and differential equations to

$$S_{lim} = k\left(H \pm H_c\right) \tag{12}$$

$$\frac{dS}{dH} = k\left(\frac{H - \frac{S}{k} \pm H_c}{2H_c}\right)^2 \tag{13}$$

$$\frac{dS}{dt} = \frac{dS}{dH}\frac{dH}{dt} \tag{14}$$

The positive root of Equation (13) is used when the external field H is increasing. Numerical behavior near $B = B_s$ is much better following the substitution. The bounds are linear in H and the slope quadratic in S and H. When numerically integrating Equation (14) only one trigonometric call is required per time step to recover the induced magnetic flux B from S. This compares to three trigonometric calls per time step when integrating Equation (10) directly, and so the substitution is expected to realize some computational gain. Sample loops generated from integrating Equation (14) using the same sinusoidal external magnetic field as used in Figure 3 are illustrated in Figure 4.

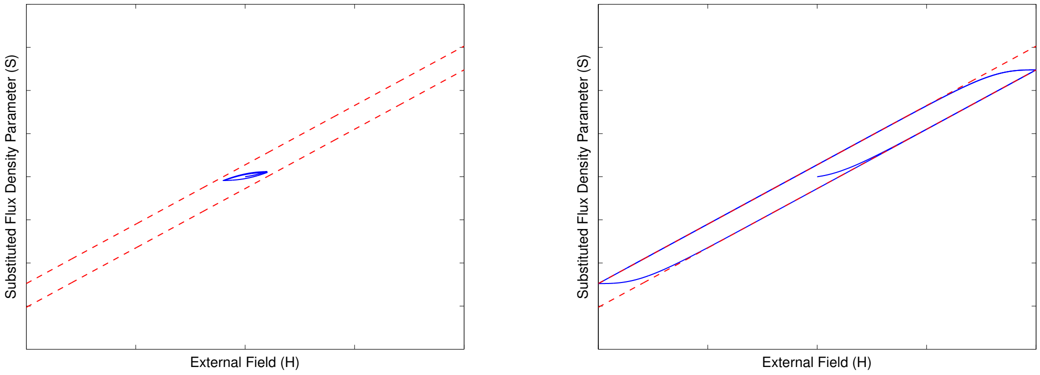

(a) $H = H_c \sin \omega t$

(b) $H = 10H_c \sin \omega t$

Figure 4. Substituted flux density loops in a sinusoidal external field

Numerical integration of the differential equation can be avoided altogether by solving Equation (13) in closed form. From an initial condition (H_0, S_0)

$$S(H) = k\left(H \pm H_c\left(1 - 2\left(\frac{1 + \alpha + \beta(\alpha - 1)}{1 + \alpha - \beta(\alpha - 1)}\right)\right)\right) \tag{15}$$

where

$$\alpha = \frac{1}{2}\left(1 \pm \frac{H_0}{H_c} \mp \frac{S_0}{2H_c k}\right) \tag{16}$$

$$\beta = \exp\left(\pm\frac{H_0 - H}{H_c}\right) \tag{17}$$

The positive root of Equations (15)–(17) is used when the external field H is increasing. The closed form solution requires no bounding steps. If the initial condition (H_0, S_0) lies within the loop, then all $S(H)$ must necessarily lie within the loop. Ideally each new (H_0, S_0) pair would occur at local extremes of H. As these are not generally known for real problems, a discretized approach is still required when implementing this method.

COMPARISON OF NUMERICAL METHODS

To compare the methods a spinning permeable rod in a constant magnetic field was simulated, as illustrated in Figure 5. The rod has volume V and inertia I, and magnetic properties H_c, B_r and B_s. The field strength is a constant H_0 and the rod starts spinning at an angular rate ω_0. The motion

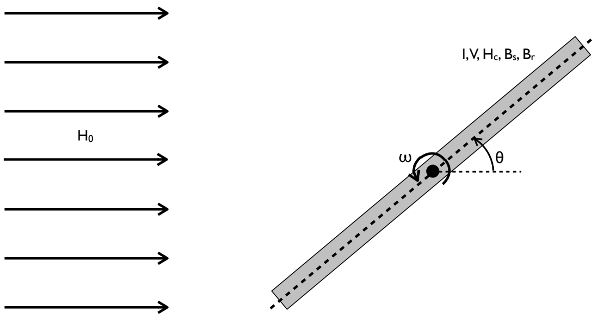

Figure 5. Spinning Rod Simulation

of the rod is described by the kinematic equation:

$$\dot{\theta} = \omega \tag{18}$$

and the dynamic equation

$$I\dot{\omega} = -BVH_0 \sin\theta \tag{19}$$

The magnetic flux in the rod B was computed using three different methods. Firstly the kinematic state $[\theta, \omega]^T$ was augmented directly with B and integrated using Equation (10). Secondly the kinematic state was augmented with S and integrated using Equation (14), with B in Equation (19) being computed at each time step from S using Equation (11). Finally B was computed directly using Equations (15) and (11) at each time step, with initial condition (H_0, S_0) being updated whenever $\dot{H}$ changed sign. In each case the states were integrated using a standard Runge-Kutta 4th order algorithm. Along the rod the external field H and its time derivative $\dot{H}$ can be computed using:

$$H = H_0 \cos\theta \tag{20}$$

$$\dot{H} = -\omega H_0 \sin\theta \tag{21}$$

Two different sets of rod parameters were examined. In both cases H_0, ω_0, I and V were held constant at 20Am^{-1}, 25°/s, 0.01kgm^2 and 17.6cm^3 respectively. The remanence and coercivity were 0.025Am^{-1} and 0.0017T respectively in the first case, and 0.8Am^{-1} and 0.06T respectively in the second case. Figure 6 compares the hysteresis loops for the two material properties simulated. Looking at the difference in areas, the second case will be expected to exhibit much faster damping. The time history of angular rate ω for the fast damping case as computed by the three different

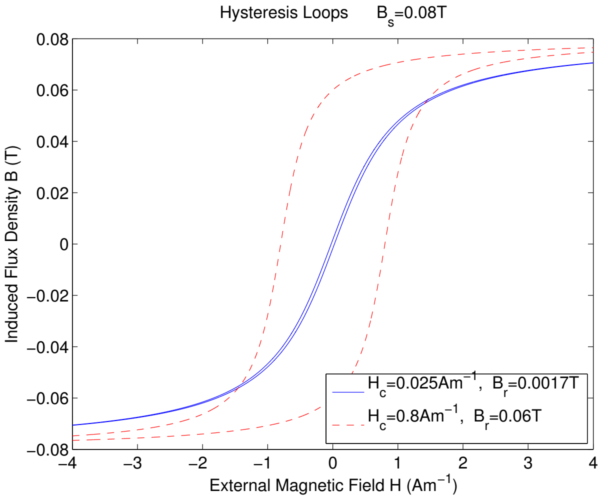

Figure 6. Comparison of Simulated Hysteresis Loops

numerical methods is shown in Figure 7(a). For the small time step shown, the three methods produce the same results to within machine precision showing numerical equivalence of the three methods.

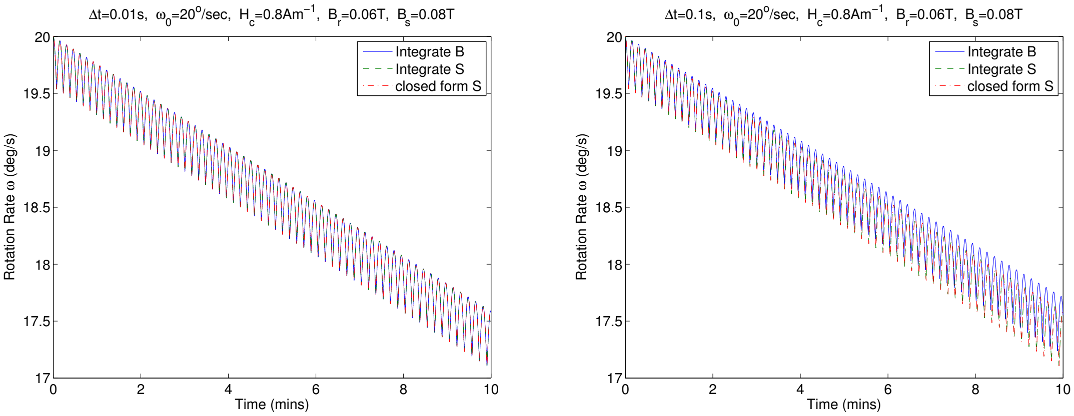

(a) Small time step

(b) Large time step

Figure 7. Sample Time History of ω

In generating Figure 7(a) the new method of integrating S took the least computational time, but was only about 20% faster than integrating B. The closed form solution was about 5% slower than direct integration of B. The real advantage of the substitution appears when the time step is increased. Figure 7(b) has the same initial conditions as Figure 7(a), but uses a time step that is ten times larger. Using this time step the direct integration of B produces different results to the other two methods indicating a divergence in numerical accuracy.

To study the numerical accuracy of the methods, convergence plots were generated and these are illustrated in Figure 8. Figure 8 plots the angular rate ω after a fixed simulation time versus the time step used for the two different damping cases. As can be seen, both the closed form solution in S and direct integration of S converge at much larger time steps, around $||\omega dt|| \approx 0.1$, compared to $||\omega dt|| \approx 0.01$ for direct integration of B. Approximately an order of magnitude larger time step can be used if integrating S rather than B, while preserving simulation accuracy. This directly translates to an order of magnitude increase in code speed as fewer steps are required to cover the same simulated time period.

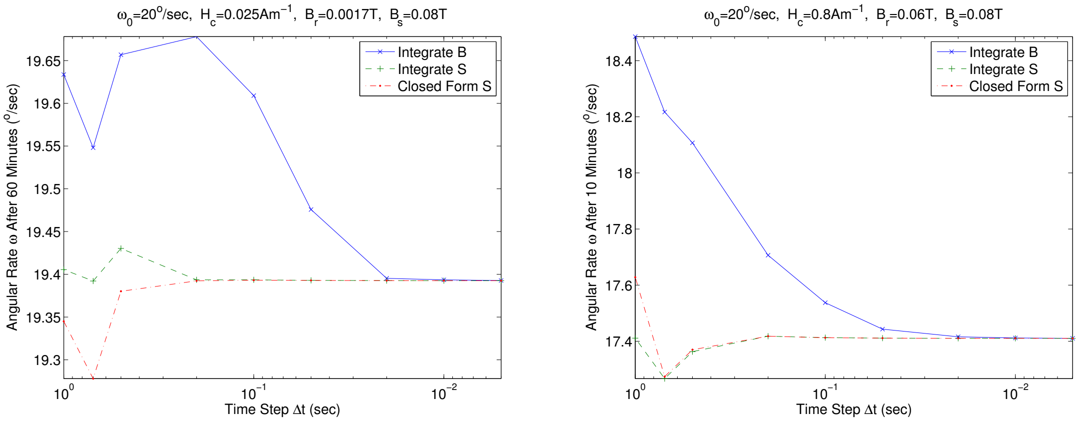

Figure 8. Comparison of Numerical Convergence

As a check of the simulation results the angular rate at the end of the simulated time period can be compared to that predicted by Equation (6). Fischell[1] showed that the damping due to hysteresis of a permeable rod spinning in a magnetic field would cause a linear decay in the angular rate:

$$\dot{\omega} = -\frac{V \oint H dB}{2\pi I} \tag{22}$$

$$= -\frac{2VB_sH_c}{\pi I} \tag{23}$$

For the the large damping case, this would lead to a decay rate of $0.25°$/s per minute, and a decrease in angular rate after ten minutes of $2.45°$/s. For small damping, the decay rate is $0.46°$/s per hour leading to a decrease in angular rate after sixty minutes of $0.46°$/s. Both of these theoretical predictions match the numerical simulation results.

APPLICATION TO O/OREOS

The Organism/Organic Exposure to Orbital Stresses (O/OREOS) spacecraft is a 3U nano satellite that launched in November 2010 from Kodiak, AK. O/OREOS carried two astrobiology payloads to study the survivability and viability of the space environment to live organisms and organics respectively. The O/OREOS spacecraft passive attitude stabilization system consisted of permanent dipoles along the long axis, and hysteresis rods in the plane perpendicular to the long axis. O/OREOS had no direct onboard attitude sensing, however the spacecraft bus did monitor solar panel currents from which characteristic spin rates can be obtained using Fourier transform techniques.

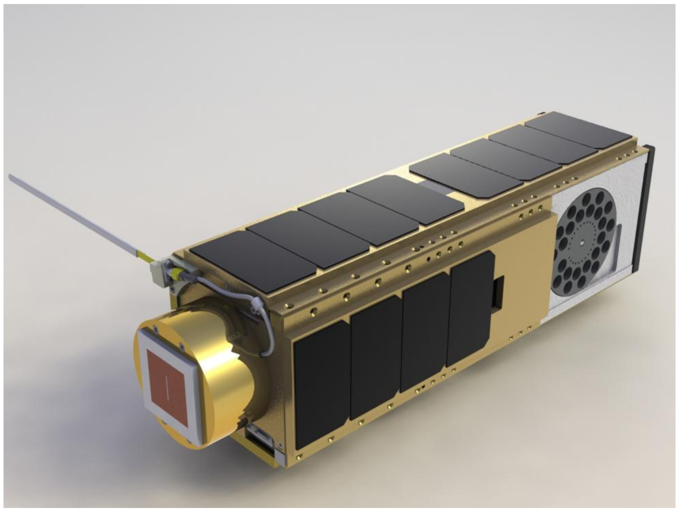

Figure 9. The O/OREOS Satellite (computer rendering)

Data Analysis

The O/OREOS satellite transmits bus data, including solar panel currents at a few different rates. The peak data sampling rate is 1Hz, although this data is not taken continuously. Data from two different time periods are shown in Figure 10.

In the first few days after launch, the longest continuous data set available was just over a minute, and Figure 10(a) is the cleanest of these early data sets. Later in the mission much longer continuous data sets were available which lasted several minutes lending more faith to the results of the Fourier analysis, such as that illustrated in Figure 10(b). As can best be estimated from the data, initial post separation spin rate was around 25°/s. Within about sixty days this had settled to around 5°/s, and stayed at this rate for the next several months. This rate matches well with the original design intent of O/OREOS which was a spin of 1-2RPM. The clean shape of the sinusoids strongly suggests that as desired the spacecraft was rotating around its long axis with little offset. Unfortunately no 1Hz data existed between weeks two and eight. Lower frequency data were available and some Lomb-Scargle Periodogram analysis was attempted on this data set, however no statistically significant results were found for the initial period in question. The lower sampling frequency of these data meant that only spin rates below 10°/s could be detected.

Lab Testing

For accurate simulation it is important to know the properties of the magnetic materials as installed in the spacecraft. Manufacturer data sheets typically quote magnetic properties to confirm with ASTM-A596,[5] which assumes an infinite length of material, as would be encountered in an annular sample of the material. For any real application involving rods of finite length, the effective damping properties of the rod are significantly reduced. Several additional factors, including rod elongation (length-to-diameter ratio), the annealing processes the rod has undergone, and the amount of cold working it has experienced can alter the rod magnetic field parameters.

To estimate the effective material properties for the O/OREOS spacecraft, a flight spare permeable rod was measured using a hysteresis characterization test procedure similar to that used by the

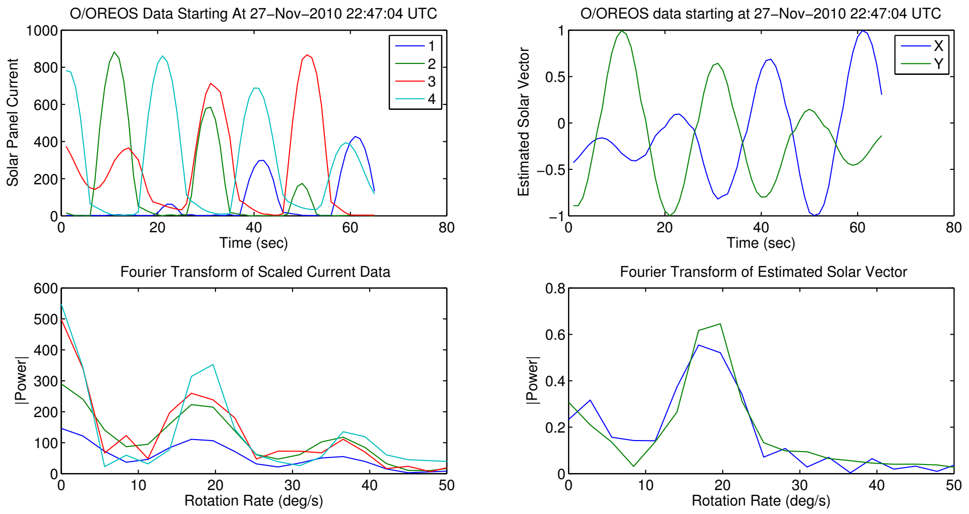

(a) A week after launch

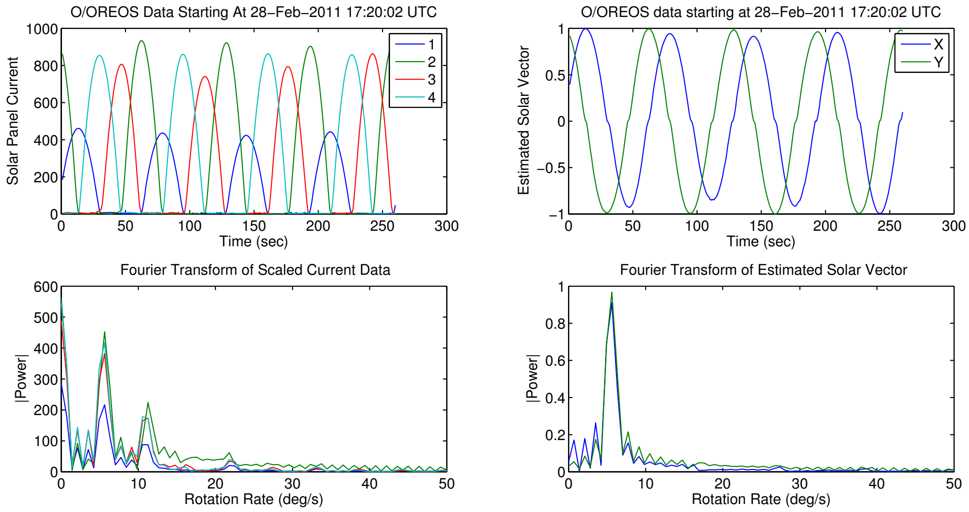

(b) Three months after launch

Figure 10. Data from two time points in the O/OROES mission

UNISAT-4 team described in Reference 6. The tests were performed at NASA Ames Research Center using the equipment illustrated in Figure 11. Hysteresis rod performance was evaluated by applying a known, constant magnetizing field to the rod and measuring the field induced. This known field was generated using a solenoid coil, whose internal magnetic field is approximately constant in magnitude and direction along its axis of symmetry at points removed from the solenoid ends. The hysteresis rod was placed inside the solenoid and the current varied to cycle the rod from negative to positive saturation and back. During this process the total external magnetic field along the shared rod and coil axis was measured some distance away. After the contributions from the solenoid itself and the Earth's field are subtracted, the magnetic flux density induced in the rod can be computed.

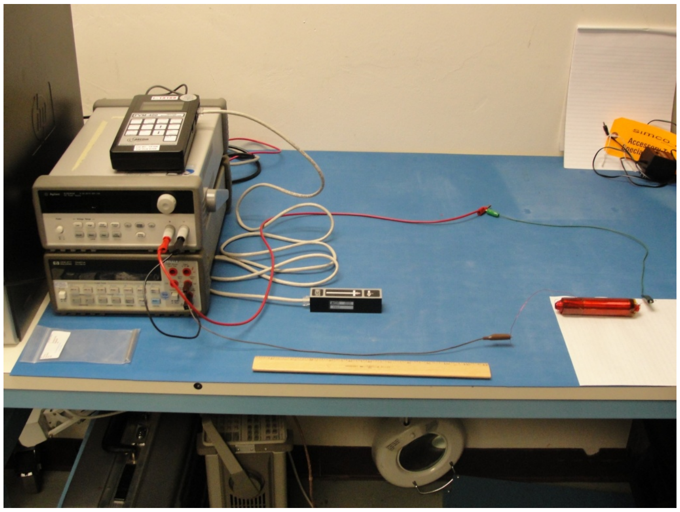

Figure 11. The Laboratory Test Equipment

The material saturation, B_s, was most easily determined and found to be 0.08T. As the hysteresis loop did not exactly match the form of the arctangent function, the coercivity, H_c, was chosen such that the observed area within the loop was equal to $4B_sH_c$, leading to a coercivity of 0.25Am^{-1}. Finally the observed remanence, B_r, was 0.0017T. The importance of taking these lab measurements becomes apparent when comparing to the manufacturers data sheet, which quotes $B_s = 1.5$T, $B_r = 0.9$T and $H_c = 4\text{Am}^{-1}$.

Full Spacecraft Attitude Model

The kinematic state of the spacecraft was represented using the unit quaternion q and the angular rates in the body frame ω. The kinematics and dynamics of the spacecraft obey

$$\dot{q} = \frac{1}{2}\omega \otimes q \tag{24}$$

$$T = I\dot{\omega} + \omega \times I\omega \tag{25}$$

Only the magnetic torque from the permanent dipoles and the hysteresis rods are considered for the analysis. Gravity gradient and aerodynamic torques are several orders of magnitude smaller than the magnetic torque and are neglected. The torque in the body frame is computed according to

$$T = M \times \mu_0 H \tag{26}$$

$$= \left(BV + 4\pi \times 10^{-7} M_{perm}\right) \times H \tag{27}$$

and the external magnetic field H and its time derivative are computed using

$$H = q \otimes H_{ECI} \otimes q^{-1} \tag{28}$$

$$\dot{H} = q \otimes \dot{H}_{ECI} \otimes q^{-1} - \omega \times H \tag{29}$$

The satellite's inertial location and velocity were computed based on O/OREOS's TLEs and a SGP4[7] propagator, and from these the external magnetic field in the ECI frame, H_{ECI}, and its time derivative, $\dot{H}_{ECI}$, were computed using the IGRF-11[8] model. In order to compute the induced magnetic flux density $B(t)$ the kinematic state was augmented with the substituted flux state S. A Runge-Kutta 4th order algorithm was used to propagate the state forward in time. In the case of torque free motion to maintain numerical stability and accuracy Equations (24) and (25) should be integrated using a time step to ensure that $||\omega dt|| < 0.1$. This time step is still suitable when magnetic torques are included in the model, and induced flux density is computed by integrating the substituted flux state S. By contrast, if the induced flux density B were to have been integrated directly, then a much smaller time step would be required to satisfy $||\omega dt|| < 0.01$ and the simulations would have taken an order of magnitude longer to run.

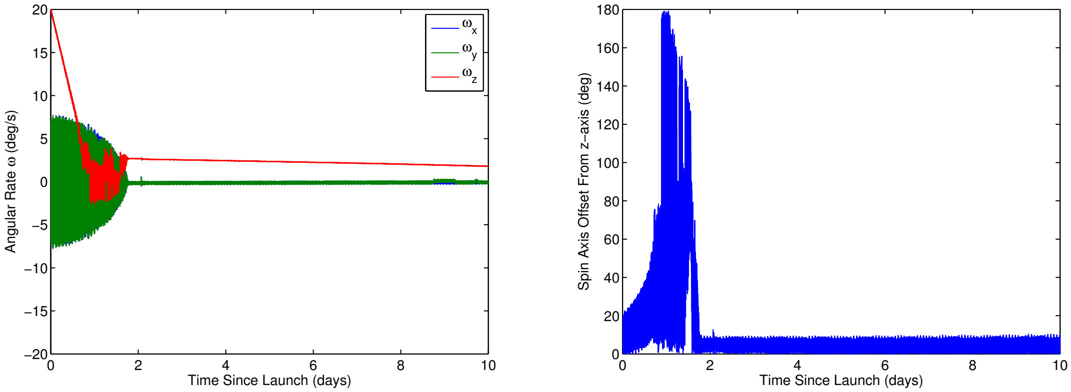

Figure 12. Sample Simulation Results for O/OREOS

Simulation Results

A sample full simulation of O/OREOS during the first ten days after separation is illustrated in Figure 12, which includes plots of the body angular rates $(\omega_x, \omega_y, \omega_z)$ and the offset of the spin axis to the spacecraft long axis (z-axis). An initial spin rate of 20°/s was assumed based on the initial rates seen from the orbital data. Initial attitude was random. The ten day simulation took under ten minutes to complete on a dual core laptop using the new integration technique. By comparison on the same hardware direct integration of B took almost 2 hours to complete.

For easier direct comparison with the orbit data, a Fourier analysis was performed based on the simulated sun vector, and this is illustrated in Figure 13. The time in the simulation chosen for the analysis was at the start of day seven, corresponding to the same time period as Figure 10(b).

While the spacecraft is principally spinning around its long axis Equation (23) can be used to predict a theoretical decay rate of $0.9°$/hr, and this is initially observed in the simulation for ω_z. The final settled angular rate in the simulation was slightly below the $5°$/s rate observed in the orbit data, and the offset of the spin axis to the long axis was less than $10°$. The much faster settling time observed in the simulation as compared to the orbit data is likely because the effective damping power of the permeable rods will be less when installed in a spacecraft as opposed to when isolated in a laboratory. These effects can only be quantified in the lab to a limited extent, but the fast simulation times now achievable will allow the effects to be explored using parameter identification techniques.

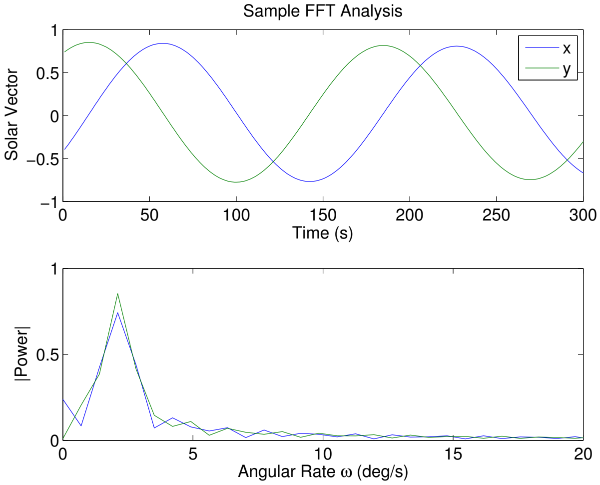

Figure 13. Fourier Analysis on Simulated Results Sun Vector

CONCLUSIONS

A new method for integrating the differential equations used to model hysteresis material has been shown to offer an order of magnitude improvement in computation speed by allowing for larger integration time steps to be used with no loss in accuracy. Order of magnitude speed improvements carry into full attitude simulations as the upper limit on time step required by the new method for numerical accuracy is approximately equal to that required by the rigid body kinematic and dynamic differential equations. The new method was integrated into a full attitude simulation of the O/OREOS and an order of magnitude decrease in simulation run time was observed. The dramatic increase in simulation speed will allow for more initial conditions or perturbations to be studied, and for the impacts of certain design parameters to be studied in further depth.

ACKNOWLEDGMENTS

The research described in this paper was funded by a grant from NASA Ames Research Center. The laboratory testing was performed under the NASA Education Associates Program. Orbital data for the O/OREOS spacecraft was provided by Santa Clara University.

NOTATION

μ_0	permeability of free space $= 4\pi \times 10^{-7}$	Hm^{-1}
H	external magnetic field, body frame	Am^{-1}
H_{ECI}	Earth's magnetic field, ECI frame	Am^{-1}
H_c	coercivity of permeable material	Am^{-1}
B	induced magnetic flux density in a permeable material	T
B_r	remanence flux density of permeable material	T
B_s	saturation flux density of permeable material	T
V	volume of permeable material	m^3
E_h	energy decay due to hysteresis	J
M	induced dipole of permeable material	Am^2
M_{perm}	permanent dipole in a permanent magnet	Am^2
I	moment of inertia, body frame	kgm^2
T	external torque, body frame	Nm
ω	angular rate, body frame	rad/s
q	unit quaternion, inertial to body frame	

REFERENCES

[1] R. Fischell, "Magnetic damping of the angular motions of earth satellites," *ARS Journal*, Vol. 31, No. 9, 1961, pp. 1210–1217.

[2] T. W. Flatley and D. A. Henretty, "A Magnetic Hysteresis Model," *Flight Mechanics/Estimation Theory Symposium 1995* (K. R. Hartman, ed.), May 1995, pp. 405–415.

[3] R. R. Kumar, M. L. Heck, and D. D. Mazanek, "Simulation and Shuttle Hitchhiker validation of passive satellite aerostabilization," *Journal of Spacecraft and Rockets*, Vol. 32, Sept. 1995, pp. 806–811, 10.2514/3.26688.

[4] G. Park, S. Seagraves, and N. H. McClamroch, "A Dynamic Model of a Passive Magnetic Attitude Control System for the RAX Nanosatellite," *AIAA Guidance, Navigation, and Control Conference, Toronto, Ontario, Aug. 2-5, 2010*, 2010, AIAA-2010-8154.

[5] ASTM, *ASTM Standard A596 / A596M - 95(2009)e1: Standard Test Method for Direct-Current Magnetic Properties of Materials Using the Ballistic Method and Ring Specimens*. West Conshohocken, PA: ASTM International, 2009.

[6] F. Santoni and M. Zelli, "Passive magnetic attitude stabilization of the UNISAT-4 microsatellite," *Acta Astronautica*, Vol. 65, No. 5-6, 2009, pp. 792 – 803, 10.1016/j.actaastro.2009.03.012.

[7] D. Vallado, P. Crawford, R. Hujsak, and T. Kelso, "Revisiting spacetrack report# 3," *AIAA*, Vol. 6753, 2006, p. 2006.

[8] International Association of Geomagnetism and Aeronomy, Working Group V-MOD. Participating members, C. C. Finlay, S. Maus, C. D. Beggan, T. N. Bondar, A. Chambodut, T. A. Chernova, A. Chulliat, V. P. Golovkov, B. Hamilton, M. Hamoudi, R. Holme, G. Hulot, W. Kuang, B. Langlais, V. Lesur, F. J. Lowes, H. Lhr, S. Macmillan, M. Mandea, S. McLean, C. Manoj, M. Menvielle, I. Michaelis, N. Olsen, J. Rauberg, M. Rother, T. J. Sabaka, A. Tangborn, L. Tffner-Clausen, E. Thbault, A. W. P. Thomson, I. Wardinski, Z. Wei, and T. I. Zvereva, "International Geomagnetic Reference Field: the eleventh generation," *Geophysical Journal International*, Vol. 183, No. 3, 2010, pp. 1216–1230, 10.1111/j.1365-246X.2010.04804.x.